Scaling law of mixing layer in cylindrical Rayleigh-Taylor turbulence

Zhiye Zhao [1,2,*] Pei Wang,[2] Nan-Sheng Liu,[1] and Xi-Yun Lu[1]

[1]*Department of Modern Mechanics, University of Science and Technology of China, Hefei, Anhui 230026, China*

[2]*Institute of Applied Physics and Computational Mathematics, Beijing 10094, China*

The nonlinear evolution of mixing layer in cylindrical Rayleigh-Taylor (RT) turbulence is studied theoretically and numerically. The scaling laws including the hyperbolic cosine growth for outward mixing layer and the cosine growth for inward mixing layer of the cylindrical RT turbulence are proposed for the first time and verified reliably by direct numerical simulation of the Navier-Stokes equations. It is identified that the scaling laws for the cylindrical RT turbulence transcend the classical power law for the planar RT turbulence and can be recovered to the quadratic growth as cylindrical geometry effect vanishes. Further, characteristic time- and length scales are reasonably obtained based on the scaling laws to reveal the self-similar evolution features for the cylindrical RT turbulence.

I. INTRODUCTION

Rayleigh-Taylor (RT) instability and its induced turbulence are of great interest in fundamentals [1,2] and applications [3,4]. Because the growth of mixing layer plays important roles in understanding the basic features of RT turbulence and designing capsules for maintaining shell integrity in inertial confinement fusion [5,6], the nonlinear evolution of the mixing layer of RT turbulence is significantly desirable to be studied in detail.

It is generally recognized that the mixing layer of planar RT turbulence evolves self-similarly and presents a quadratic growth, i.e., $h_i = \alpha_i A_T g t^2$, where $i = b, s$, h_b is the bubble mixing width, h_s is the spike mixing width, α_i is a dimensionless coefficient, $A_T \equiv (\rho_h - \rho_l)/(\rho_h + \rho_l)$ (with ρ_h and ρ_l being the heavy and light fluid density, respectively) is the Atwood number, g is the magnitude of external acceleration **g**, and t is time. This self-similar modal growth was first exploited by Youngs [7] to describe the RT turbulent mixing layer growth. Then the quadratic growth was also obtained by Ristorcelli and Clark [8] and Cook *et al.* [9] based on the similarity assumption and mass flux argument, respectively. Recently, as indicated in the review articles [5,6], the quadratic scaling relation with time for the mixing layer of planar RT turbulence was also supported by extensive experiments [10–13] and simulations [14–20].

Convergence geometries occur usually in practical cases, such as inertial confinement fusion [3,21] and supernova explosions [4,22]. Principal effects of convergence geometries on the RT instability can be involved in a canonical cylindrical system [23–25]. Also the cylindrical geometry has been usually employed in experiments, as the perturbation growth of the RT instability can be conveniently measured along the axial direction [26,27]. Thus, a cylindrical system has been widely used as a natural choice to study the convergence effects on the RT intability growth [23–32]. According to the analytical model derived in our recent work [32], the cylindrical RT instability is indicated to have striking difference from its planar counterpart, as it obtains the bubble acceleration saturation behavior other than the velocity saturation as found in planar geometry. However, there is still never any work to investigate the nonlinear evolution of cylindrical RT turbulent mixing layer under the general multimode influence.

In the present study, the nonlinear evolution of mixing layer in cylindrical RT turbulence is studied theoretically and numerically. The scaling law of mixing layer in cylindrical RT turbulence was proposed for the first time and verified by direct numerical simulation (DNS) of the Navier-Stokes equations. The remainder of this paper is organized as follows. The DNS strategy for verifying the scaling law is described in Sec. II. General features of the cylindrical RT turbulence are investigated in Sec. III. The scaling law of turbulent mixing layer growth is derived and the relevant results are discussed in Sec. IV. Finally, the conclusions are addressed in Sec. V.

II. NUMERICAL SIMULATIONS

A. Governing equations and numerical method

DNS has been performed on the RT turbulence in cylindrical geometry to study the nonlinear evolution behaviours of turbulent mixing layer. Considering the cylindrical coordinates (r, θ, z), the initial pressure p_I, and density $\rho_I = (\rho_h + \rho_l)/2$ at the heavy or light fluid interface are chosen as the characteristic scales, where ρ_h and ρ_l are the heavy and light fluid density. Then the characteristic velocity and temperature are presented as $U_I = \sqrt{p_I/\rho_I}$ and $T_I = p_I/(R\rho_I)$ with the perfect gas constant R, respectively. The radius of the unperturbed interface r_0 is used as the characteristic

---

*Corresponding author: zzy12@ustc.edu.cn

length. Then the nondimensionalized governing equations are given as

$$\frac{\partial \rho}{\partial t} + \nabla \cdot (\rho \mathbf{u}) = 0, \qquad (1)$$

$$\frac{\partial (\rho \mathbf{u})}{\partial t} + \nabla \cdot (\rho \mathbf{u}\mathbf{u}) = -\nabla p + \frac{1}{\mathrm{Re}} \nabla \cdot \boldsymbol{\tau} - \frac{\rho}{\mathrm{Fr}} \widehat{\mathbf{e}}_r, \qquad (2)$$

$$\frac{\partial (\rho E)}{\partial t} + \nabla \cdot [(\rho E + p)\mathbf{u}]$$
$$= \frac{1}{\mathrm{Re}} \nabla \cdot (\boldsymbol{\tau} \cdot \mathbf{u}) + \frac{1}{\mathrm{RePr}} \nabla \cdot (\nabla T) - \frac{\rho}{\mathrm{Fr}} \mathbf{u} \cdot \widehat{\mathbf{e}}_r, \qquad (3)$$

where t, $\mathbf{u} = [u_r, u_\theta, u_z]$, ρ, p, T, and $E = T/(\gamma - 1) + \mathbf{u} \cdot \mathbf{u}/2$ denote the time, velocity, density, pressure, temperature, and total energy, respectively, where $\gamma = 1.4$ is the specific heat ratio and $\widehat{\mathbf{e}}_r$ is the unit vector in the radial direction. The stress tensor is obtained as

$$\boldsymbol{\tau} = 2\mu \mathbf{S} - \tfrac{2}{3}\mu(\nabla \cdot \mathbf{u})\boldsymbol{\delta}, \qquad (4)$$

where $\mathbf{S}$ is the strain-rate tensor, $\boldsymbol{\delta}$ is the unit tensor, and $\mu = T^{3/2}(1 + c)/(T + c)$ is the viscosity calculated by the Sutherland law with $c = 110/T_r$ and the reference temperature T_r.

The nondimensional parameters in Eqs. (1)–(3), i.e., the Reynolds, Froude, and Prandtl numbers, are defined as, respectively,

$$\mathrm{Re} = \frac{\rho_I U_I r_0}{\mu_I}, \quad \mathrm{Fr} = \frac{U_I^2}{r_0 g}, \quad \text{and} \quad \mathrm{Pr} = C_p \frac{\mu_I}{\kappa}, \qquad (5)$$

where g is the external acceleration, C_p the constant-pressure specific heat, and κ the thermal conductivity.

We have developed the in-house program code with high-order accuracy schemes to solve the compressible Navier-Stokes equations in cylindrical coordinate for the performance of cylindrical RT turbulence. Our program code has been successfully used to simulate the cylindrical RT instability and RT turbulence in our recent work [20,32]. The seventh-order finite difference WENO scheme is implemented to discretize the convective terms and the eighth-order central difference scheme to discretize the viscous terms of the governing Eqs. (1)–(3). The time derivatives are approximated by the standard third-order Runge-Kutta method.

B. Flow-field initialization and numerical details

The cylindrical RT turbulence is driven by an external acceleration imposed pointing from the heavy to the light fluid as shown in Fig. 1. Because there are two classes of RT unstable systems in cylindrical geometry, one comprises the heavy fluid surrounding the light fluid and the other comprises the light fluid surrounding the heavy fluid, and thus the cylindrical RT instability can be classified into a convergent case [see Fig. 1(a)] and a divergent case [see Fig. 1(b)] based on the direction of external acceleration [29], and for both cases the flow fields are initialized as follows. To avoid the instability suppression due to background stratification, uniform density field is initialized as $\rho_h = 1 + A_T$ and $\rho_l = 1 - A_T$ on each side of the interface [32–34], where the Atwood number $A_T \equiv (\rho_h - \rho_l)/(\rho_h + \rho_l)$. The initial velocity field is set to be zero. The hydrostatic equilibrium requires that
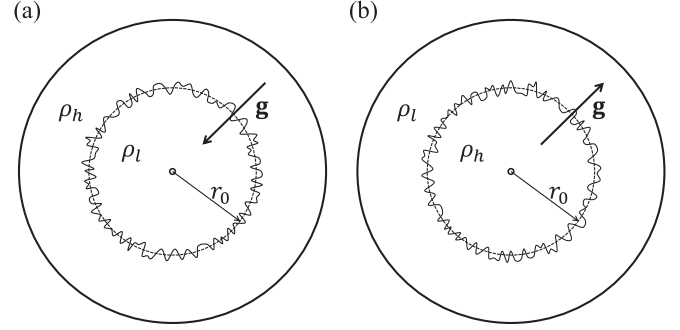

FIG. 1. The diagram of cylindrical RT instability for (a) convergent case and (b) divergent case.

$dp/dr = -\rho_i/\mathrm{Fr}$ $(i = l, h)$ away from the interface, thus the pressure field can be determined by assuming $p = 1$ at the interface.

To stimulate the fully developed cylindrical RT turbulence, the interface at $r_0 = 1$ is perturbed by introducing small disturbance given as $\sum_{n,k_z} A_m \cos(n\theta + \varphi_n)\cos(2\pi k_z z/L_z + \psi_z)$, where the amplitude $A_m = 3 \times 10^{-4}$ for the three-dimensional (3D) cases and $A_m = 10^{-3}$ for the 2D cases, the perturbation wave numbers n and k_z in the circumferential and axial direction are set in a range of $30 \leqslant \sqrt{n^2 + k_z^2} \leqslant 60$, the axial length $L_z = 2\pi$, φ_n, and ψ_z are random phases [20,35]. The velocity, pressure, and density at the far boundary are fixed as their initial values to ensure hydrostatic equilibrium [32,36]. The RT flow is considered to be homogeneous in the z direction thus along which periodic boundary conditions are used for the 3D simulations.

To verify the scaling law of RT turbulent mixing layer, various simulation parameters as listed in Table I have been selected for convergent (i.e., the external acceleration $\mathbf{g}$ acting radially inward) and divergent (i.e., $\mathbf{g}$ acting radially outward) cases in the present study. The Prandtl number of all cases is selected as $\mathrm{Pr} = 0.72$ for air. In the present simulations, to avoid a pole singularity at the center of cylindrical coordinate, the inner boundary at a small radius $r_{\min} = 0.05$ has been used with the zero gradient boundary conditions, following the previous treatment [32,37,38]. The radial grids are set as $r_{i+1} = r_i(1 + \Delta\theta)$, where r_i is the radial position of the ith grid and the width of uniform circumferential girds $\Delta\theta =$

TABLE I. Simulation parameters for DNS. The outer scale Reynolds number, based on the visual width H corresponding to a layer where the mole fraction of heavy fluid averaged in θ-z plane falls between 1% and 99%, is defined as $\mathrm{Re}_H = \rho_I H \dot{H}/\mu_I$ [16].

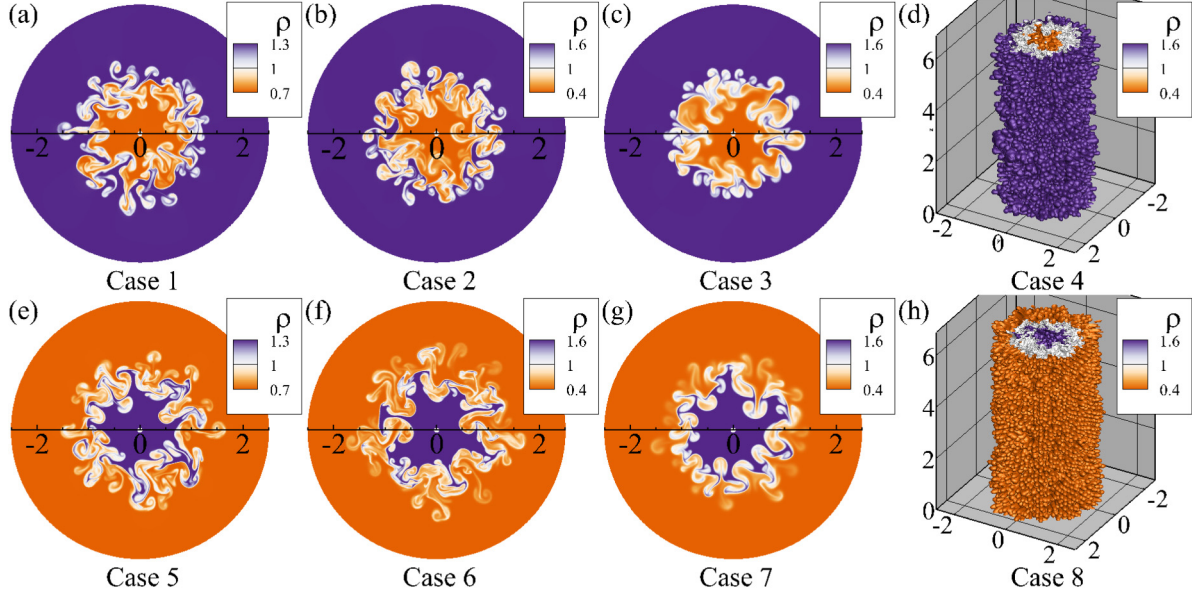| Cases	Direction of **g**	A_T	Re	Fr	Dimension	Re_H
1	Convergent	0.3	40 000	10	2D	13 600
2	Convergent	0.6	40 000	10	2D	14 200
3	Convergent	0.6	20 000	20	2D	5800
4	Convergent	0.6	40 000	10	3D	13 000
5	Divergent	0.3	40 000	−10	2D	12 500
6	Divergent	0.6	40 000	−10	2D	14 500
7	Divergent	0.6	20 000	−20	2D	5300
8	Divergent	0.6	40 000	−10	3D	15 300

FIG. 2. Snapshots of instantaneous density fields for 2D convergent (a)–(c) and divergent (e)–(g) cases at the rescaled time $\tau = 3$. Isosurfaces of the density (orange for $\rho = 0.41$, gray for $\rho = 1$, and purple for $\rho = 1.59$) for 3D convergent (d) and divergent (h) cases at the rescaled time $\tau = 3$.

$2\pi/N$, and the axial grids are uniform. The 2D cases in Table I are calculated by use of 1000 and 1600 grids in the radial and circumferential direction, and the 3D cases are calculated by 500, 800, and 800 grids in the radial, circumferential, and axial directions, respectively, which have been verified to reliably resolve the flow scales [32].

III. PHYSICAL FEATURES

The multiscale feature, self-similarity, mixing width, and fundamental measurements of mixing layer for cylindrical RT turbulence are examined by means of DNS in this subsection.

A. Multiscale feature of turbulent mixing layer

The instantaneous density fields at turbulent stage are shown in Fig. 2 for all the cases listed in Table I. It exhibits fine-scale structures and large patches of mixed fluids. Specifically, large-scale structures are well identified in the turbulent mixing layer, which arise due to the merging of bubbles and spikes. Small-scale structures are also fully visible along the evolutional interface between heavy and light fluids. This visualization indicates clearly the multiscale feature of RT turbulence [8,16,39].

Moreover, the density spectra are defined by

$$E_\rho(r, k_\theta, t) = \widehat{\rho'}^{*} \widehat{\rho'}(r, k_\theta, t), \quad (6)$$

where k_θ is the wave number in the circumferential direction, $\widehat{\rho'}$ is the Fourier transformation of the density fluctuation, and $\widehat{\rho'}^{*}$ is its complex conjugate. Here all the density spectra are calculated at $r_0 = 1$ and normalized by integrated density spectra $E_{tot} = \int E_\rho \, dk_\theta$. The energy spectra of cases 4 and 8 are averaged in the axial direction. As shown in Fig. 3 for the density spectra in the circumferential direction, where the abscissas are scaled as $k_\theta r_0$, not only the scales of initial
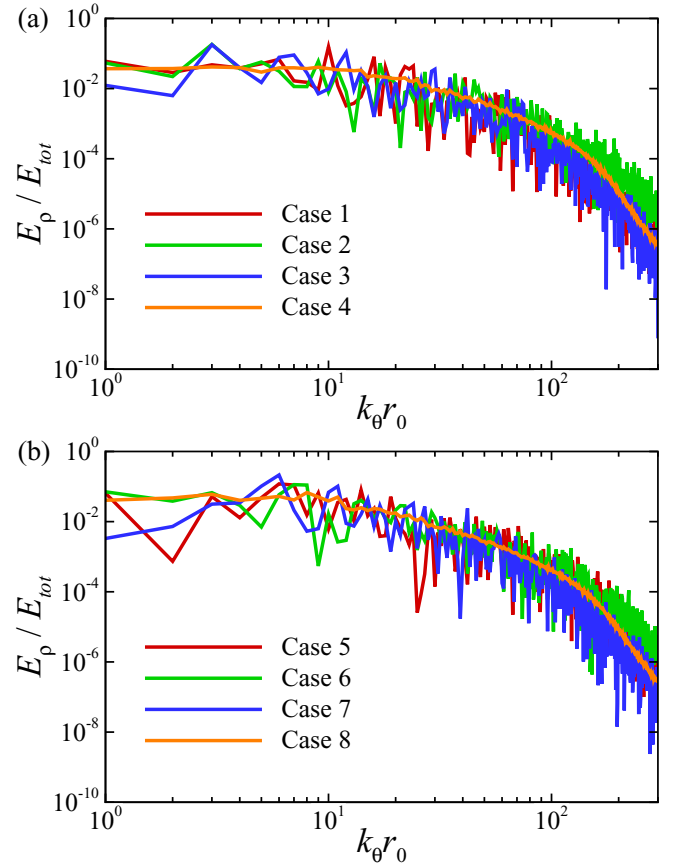

FIG. 3. The density energy spectra in the circumferential direction at $r_0 = 1$ for (a) convergent and (b) divergent cases at the rescaled time $\tau = 3$. The energy spectra of cases 4 and 8 are obtained by an average in the axial direction.
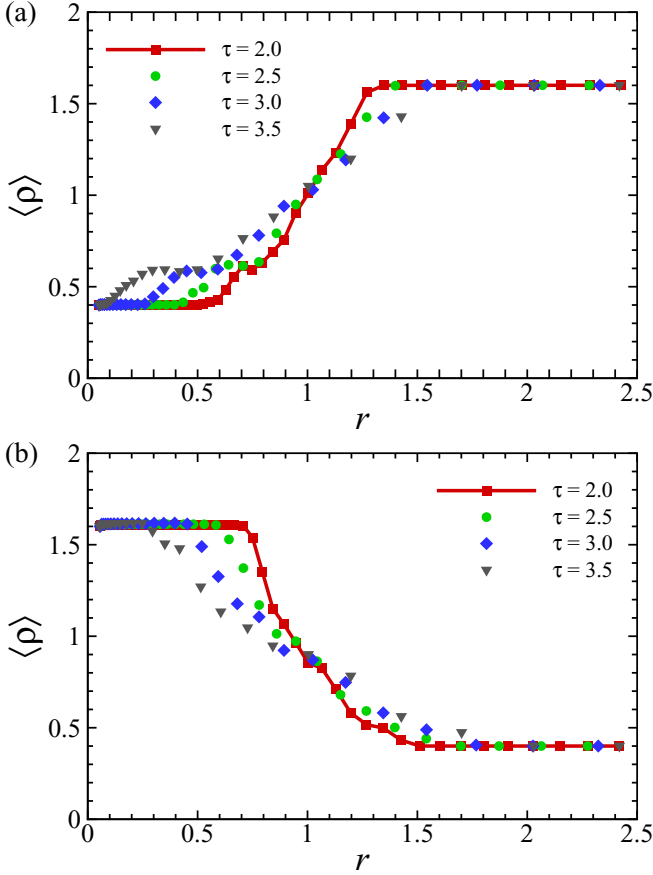
FIG. 4. Mean density distributions in the radial direction for the typical cases at different moments: (a) case 2 and (b) case 6.

FIG. 5. Mean density distributions versus similarity variable ξ for typical cases at different moments: (a) case 2 and (b) case 6.

perturbation (i.e., $30 \leqslant k_\theta \leqslant 60$) but also a wide range of scales are excited in the flows due to the nonlinear interaction of bubbles and spikes, and thus the flows reach turbulent stage.

Furthermore, to assure that the cylindrical RT flows satisfy the mixing transition criterion (Reynolds number $>1 \times 10^4$) [40] and the minimum state criterion (Reynolds number $>1.6 \times 10^5$) [41], the outer scale Reynolds number [16] calculated at the end of simulation time have been listed in Table I, demonstrating that Re_H reaches the order of 10^4 for the cases with $\mathrm{Re} = 40\,000$. Therefore, the cylindrical RT flows do not meet the minimum state criterion of Zhou [41] to reproduce the spectral range corresponding to an astrophysical event. Nevertheless, the simulated flows satisfy the transition criterion of Dimotakis [40] to reflect the beginning of the formation of the inertial range, namely the turbulent states have been achieved [16].

B. Self-similarity of turbulent mixing layer

The self-similarity is another feature of RT turbulence, which can be analyzed by the mean density distribution across the mixing layer. The mean density distributions in the radial direction for case 2 and case 6 have been shown in Fig. 4. It is seen that the mean density distributions along the radial direction become smoother as the time increases, indicating an increase of mixing width. However, the mean density distributions at different moments has the same radial
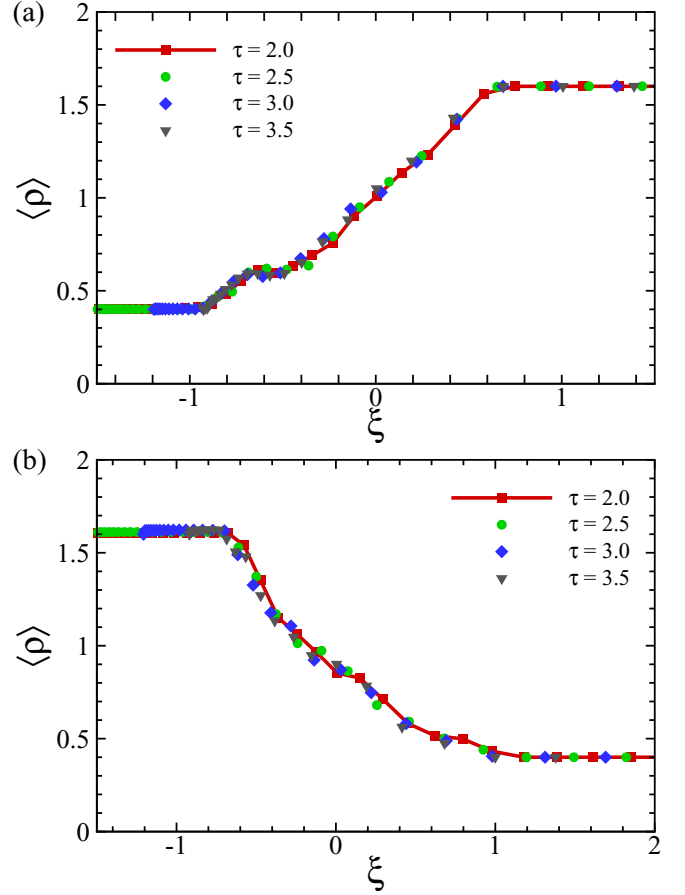
variation trend, indicating that cylindrical RT turbulence is self-similar. To this end, the mean density distribution can be represented as

$$\langle \rho \rangle (r,t) = \rho_0 F_\rho(\xi), \quad \xi = \frac{r - r_0}{h(t)}, \tag{7}$$

where ρ_0 is the scaling coefficient, $F_\rho(\xi)$ is the spatial similarity function, and h is the width of mixing layer defined as the sum of the mean widths of inward and outward mixing layers [20,39], i.e., $h_{\mathrm{in}} = 4 \int_0^{r_0} \langle X \rangle (1 - \langle X \rangle) \, dr$ and $h_{\mathrm{out}} = 4 \int_{r_0}^{\infty} \langle X \rangle (1 - \langle X \rangle) \, dr$, where X is the mole fraction of the heavy fluid defined as $X = (\rho - \rho_l)/(\rho_h - \rho_l)$ and $\langle \rangle$ denotes the spatial average in the θ-z plane.

Figure 5 shows the mean density distributions versus the similarity variable ξ for cases 2 and 6. It is clearly seen that the mean density distributions at different instants nearly collapse into a single curve. This behavior also means that the cylindrical RT flow achieves turbulent phase with self-similarity [5] and a scaling law may exist to describe the mixing layer growth.

C. Mixing width and mixed mass of turbulent mixing layer

The width of mixing layer h is a fundamental measurement of RT turbulence and thus we examine the temporal evolution of the mixing width in cylindrical RT turbulence, as shown
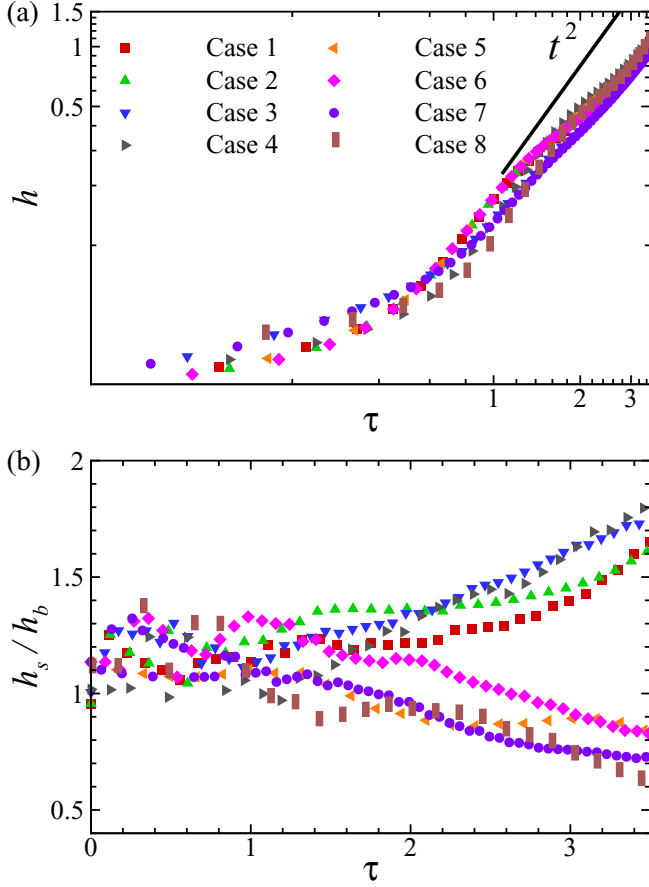
FIG. 6. Temporal evolution of (a) the width of mixing layer h and (b) the ratio of width of spike region to that of bubble region, h_s/h_b, for the cases listed in Table I.

FIG. 7. Temporal evolution of (a) the mixed mass M and (b) the normalized mixed mass Ψ for the cases listed in Table I.

in Fig. 6(a). It is seen that the mixing layer growth of the cylindrical RT turbulence, unlike its planar counterpart [8,9], do not obviously scale as t^2 at late times, which prompted us to propose a novel scaling law of mixing layer in cylindrical RT turbulence. Moreover, the ratio of width of spike region to that of bubble region, h_s/h_b, has been shown in Fig. 6(b). For the convergent cases that inward mixing layer is the spike region (i.e., $h_s = h_{\text{in}}$), h_s/h_b reaches 1.6 at late times for the cases $A_T = 0.6$ ($\rho_h/\rho_l = 4$), which exceeds the counterpart value of planar RT turbulence [6,18]. For the divergent cases that inward mixing layer is the bubble region (i.e., $h_b = h_{\text{in}}$), most interestingly, h_s/h_b is less than 1 at late times for all the cases listed in Table I. The above observations demonstrate clearly the effects of cylindrical geometry on mixing layer, specifically, the inward growth of the mixing layer is enhanced by the cylindrical effects.

The mixed mass and normalized mixed mass [42] are also fundamental measurements that have been developed specifically for hydrodynamic instabilities mixing. The mixed mass M is defined as follows [42]:

$$M = 4 \int \rho Y_1 Y_2 dV, \qquad (8)$$

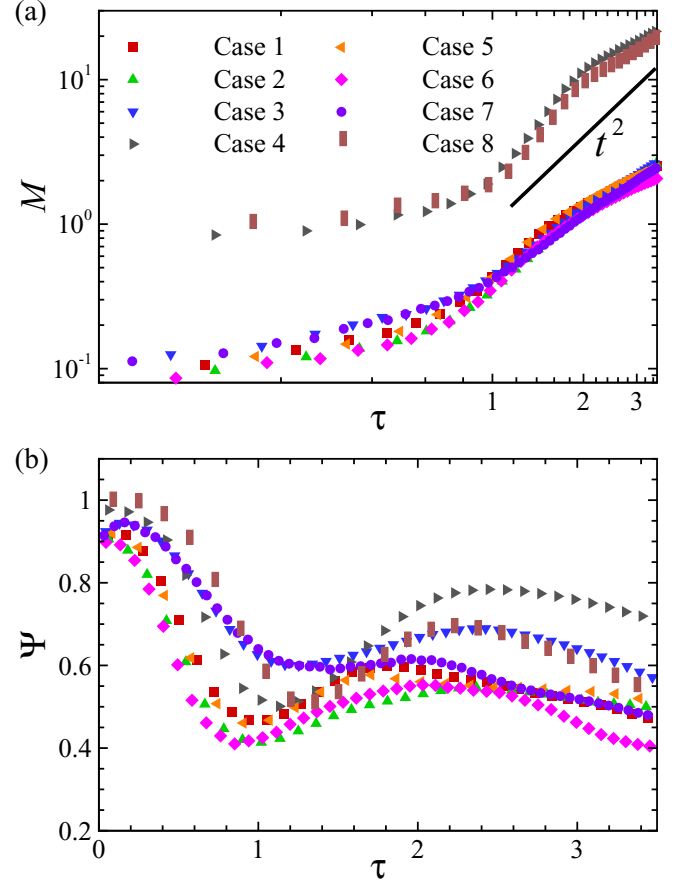where ρ denotes the density of mixture, V denotes the volume of mixing region, and Y_1 (Y_2) denotes the mass fraction of

heavy (light) fluid. As shown in Fig. 7(a), the mixed mass increases with time as the increase of mixing width, which is the same as the results of the planar RT flows [42]. However, different from the planar RT flows [42], the mixed mass curves in cylindrical RT turbulence do not scale as t^2. Because the RT flow evolutions have a dependence on the direction of external acceleration in cylindrical geometry, there exist differences in the mixed mass between convergent cases (cases 1–4) and divergent cases (cases 5–8), especially at late times.

Furthermore, the normalized mixed mass is defined as follows [42]:

$$\Psi = \int \rho Y_1 Y_2 dV / \int \langle \rho \rangle \langle Y_1 \rangle \langle Y_2 \rangle dV. \qquad (9)$$

It is plotted in Fig. 7(b) as a measurement of the efficiency of mass mixing. Similarly to the planar results [42], the normalized mixed mass curves also have valleys for cylindrical geometry at early times about $\tau = 1.1$. However, these curves show no obvious asymptotic behaviors for cylindrical geometry in this study. Moreover, the normalized mixed mass has a dependence on the direction of external acceleration in cylindrical geometry.

According to the above observations, the cylindrical geometry have a significant effect on the mixing evolution of RT turbulence. To this end, we propose to derive the scaling law of mixing layer in cylindrical RT turbulence.
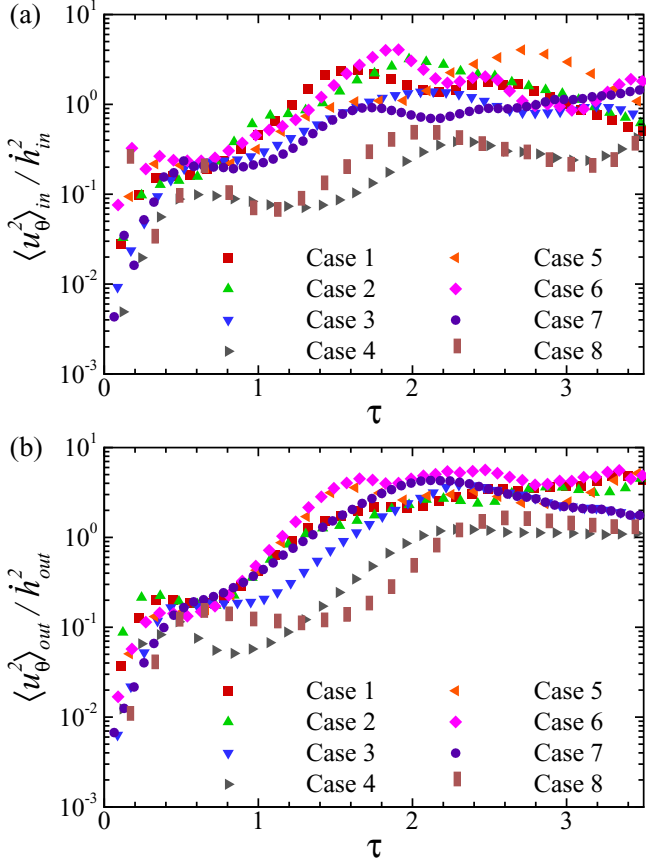
FIG. 8. Ratios of the square values of the circumferential velocity and growth velocity versus rescaled time for (a) the inward mixing layer and (b) the outward mixing layer.

IV. SCALING LAWS

We consider the mixing layer in cylindrical RT turbulence with initial perturbed interface r_0. The uniform external acceleration is imposed as $\mathbf{g} = -g\widehat{\mathbf{e}}_r$ for convergent case and $\mathbf{g} = g\widehat{\mathbf{e}}_r$ for divergent case. As the mixing region on both the sides of interface r_0 is asymmetric about the initial perturbed interface, the inward and the outward mixing layer widthes, i.e., h_{in} and h_{out}, are needed to be modelled separately.

In order to establish the scaling law of mixing layer in cylindrical RT turbulence, we first analyze the dynamic factor that govern the mixing layer growth when the flow achieves self-similarity. The basic mechanism of RT turbulence is a buoyancy-induced fluid-mixing mechanism [43]. For planar RT turbulence, if the mixing is self-similar, then the growth of the mixing layer can be modelled by [5,15]

$$\frac{d\dot{h}_i}{dt} = 2\alpha_i A_T g, \qquad (10)$$

where $i = b, s$, h_b is the bubble mixing width, h_s is the spike mixing width, and α_i denotes the dimensionless coefficient. In cylindrical RT turbulence, the outward mixing layer is the bubble region (i.e., $h_{out} = h_b$) and the inward mixing layer is the spike region (i.e., $h_{in} = h_s$) for the convergent case and vice versa for the divergent case. Equation (10) for the growth
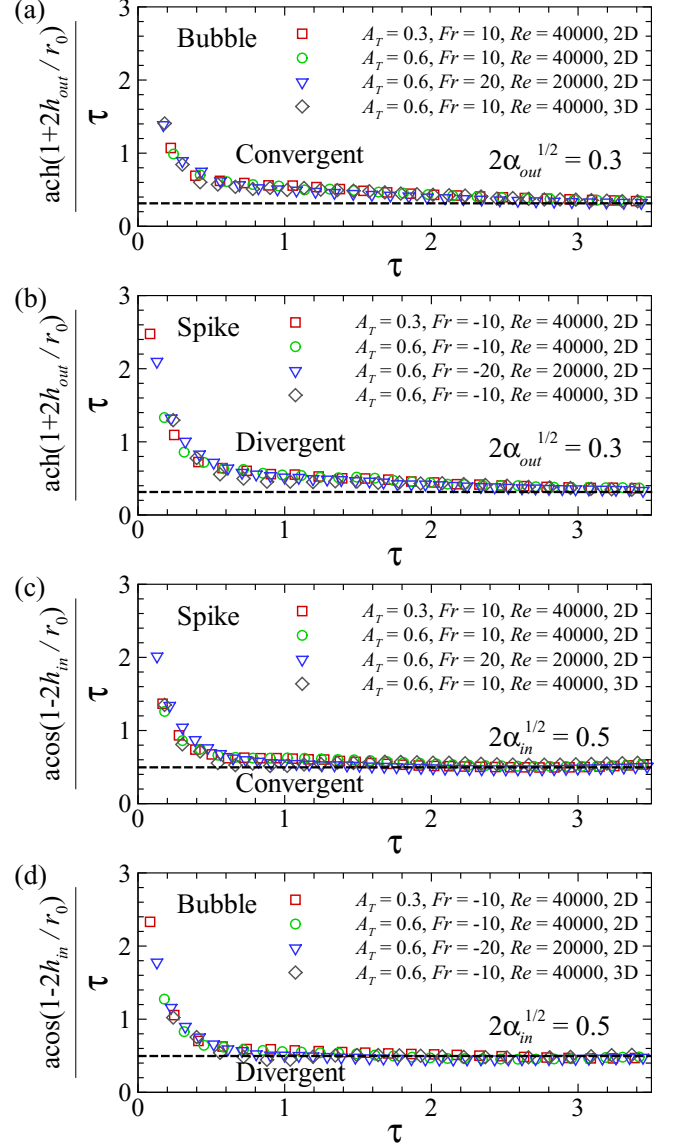

FIG. 9. The scaling law of outward mixing layer for (a) convergent cases and (b) divergent cases, and the scaling law of inward mixing layer for (c) convergent cases and (d) divergent cases.

of the mixing layer in planar RT turbulence can be outlined as follows. The advancement of the bubbles and spikes in the respective pure fluids may be viewed as the result of a buoyancy force scaled by the density difference [15]. Specifically, the left-hand-side term of Eq. (10) represents the acceleration of the mixing region, which can also be referred to as the acceleration of the fluid parcels [15], and the right-hand-side term denotes the integrated buoyancy force acting on the fluid parcels in the mixing region.

As for cylindrical RT turbulence, the evolution of the bubbles and spikes in the respective pure fluids can also be viewed as the result of a buoyancy force, which has a similar form as Eq. (10) in planar RT turbulence when scaled by density difference. In addition to the dynamic factor (i.e., radial buoyancy force), the kinematic relationship of the mixing layer growth must be considered. Therefore, the radial acceleration

of the fluid parcels in the mixing layer is obtained as

$$a_r = \frac{du_r}{dt} - \frac{u_\theta^2}{r}. \tag{11}$$

Note that the radial velocity u_r in the mixing layer determines the evolution of the mixing layer and the average magnitude of u_r is approximated as the mixing layer growth velocity, $\dot{h}_{in}$ and $\dot{h}_{out}$. Doubtlessly, when the flow reaches turbulent phase, the circumferential motion will arise due to the nonlinear effect, which is formulated as the term u_θ^2/r that also contributes to the radial acceleration and in turn the mixing layer growth. In order to quantitatively determine the contribution of circumferential motion, employing the DNS results, the ratios, i.e., $\langle u_\theta^2 \rangle_{in}/\dot{h}_{in}^2$ and $\langle u_\theta^2 \rangle_{out}/\dot{h}_{out}^2$ for the inward and outward mixing layers, respectively, have been plotted in Fig. 8. It is exhibited clearly that u_θ in mixing layers have the same order in magnitudes with $\dot{h}_{in}$ and $\dot{h}_{out}$ at $\tau \gtrsim 2.0$ when the flows achieve turbulent state. In that u_θ^2/r is reasonably estimated as $\dot{h}_{out}^2/r_{out}$ for the outward mixing layer and $\dot{h}_{in}^2/r_{in}$ for the inward mixing layer, where $r_{out} = r_0 + h_{out}$ and $r_{in} = r_0 - h_{in}$ are the mean radii of outward and inward mixing layers, respectively. Thus, considering the growth of mixing layer caused by buoyancy force, the model equations of the inward and outward mixing layers in cylindrical RT turbulence can be derived, given as

$$\frac{d\dot{h}_{in}}{dt} + \frac{\dot{h}_{in}^2}{r_0 - h_{in}} = 2\alpha_{in}A_T g, \tag{12}$$

and

$$\frac{d\dot{h}_{out}}{dt} - \frac{\dot{h}_{out}^2}{r_0 + h_{out}} = 2\alpha_{out}A_T g, \tag{13}$$

respectively, where α_{in} and α_{out} are dimensionless coefficients. As expected, when the effect of cylindrical geometry becomes negligibly weak as $r_0 \to \infty$, both Eqs. (12) and (13) for the cylindrical RT mixing layer are reduced straightforwardly to Eq. (10) for the planar RT mixing layer.

Here Eqs. (12) and (13) are nonhomogeneous and can be solved by the method of constant variation. Integrating the homogeneous parts of Eqs. (12) and (13) gives $\dot{h}_{in} = C_{in}(r_0 - h_{in})$ and $\dot{h}_{out} = C_{out}(r_0 + h_{out})$, where C_{in} and C_{out} are integral constants. We assume that $\dot{h}_{in} = C_{in}(t)(r_0 - h_{in})$ and $\dot{h}_{out} = C_{out}(t)(r_0 + h_{out})$ are solutions of Eqs. (12) and (13), which lead to $C_{in}(t) = 2[\alpha_{in}A_T g/(r_0 - h_{in}) - \alpha_{in}A_T g/r_0]^{1/2}$

and $C_{out}(t) = 2[\alpha_{out}A_T g/r_0 - \alpha_{out}A_T g/(r_0 + h_{out})]^{1/2}$ when substituting into Eqs. (12) and (13) for a subsequent integrating. Finally, as the initial mixing widths are zero, the widths of the inward and outward mixing layers can be obtained by integrating $\dot{h}_{in} = C_{in}(t)(r_0 - h_{in})$ and $\dot{h}_{out} = C_{out}(t)(r_0 + h_{out})$,

$$\frac{h_{in}}{r_0} = \frac{1}{2}(1 - \cos 2\sqrt{\alpha_{in}}\tau), \tag{14}$$

and

$$\frac{h_{out}}{r_0} = \frac{1}{2}(\cosh 2\sqrt{\alpha_{out}}\tau - 1), \tag{15}$$

where $\tau = (A_T g/r_0)^{1/2}t$ is the rescaled time. Based on the scaling law, $(r_0/A_T g)^{1/2}$ and r_0 are taken as a natural choice of the characteristic time- and length scales for the self-similar evolution of the cylindrical RT turbulent mixing layer.

In the following, we employ the high-fidelity DNS results obtained for the cases of cylindrical RT turbulence listed in Table I to verify the scaling laws described as Eqs. (14) and (15). It is exhibited in Fig. 9 that $\mathrm{acos}(1 - 2h_{in}/r_0)/\tau$ for the inward mixing layer and $\mathrm{ach}(1 + 2h_{out}/r_0)/\tau$ for the outward mixing layer expectedly tend to be a quasisteady value at $\tau \gtrsim 2.0$ for all the cases listed in Table I when the flows achieve turbulent state, which verifies that the scaling laws derived are reliable. Moreover, the symbols of all the cases in Fig. 9 collapse together excellently well, which means that the self-similar evolution features of the mixing layer in cylindrical RT turbulence are unified based on the characteristic timescale $(r_0/A_T g)^{1/2}$ and length scale r_0. Furthermore, the dimensionless coefficients α_{in} and α_{out} are given by $2\alpha_{in}^{1/2} = \mathrm{acos}(1 - 2h_{in}/r_0)/\tau$ and $2\alpha_{out}^{1/2} = \mathrm{ach}(1 + 2h_{out}/r_0)/\tau$, respectively, when $\tau \gtrsim 2.0$. Therefore, the dimensionless coefficients α_{out} and α_{in} are obtained approximately as 0.022 and 0.063 based on our DNS, falling into the range of ∼0.020-0.087 for the coefficients α_b and α_s in the planar RT turbulence [5].

Further, we can confirm that the scaling laws for cylindrical RT turbulence, i.e., the hyperbolic cosine growth of the outward mixing layer and the cosine growth of the inward mixing layer, can be reduced to the quadratic growth for planar RT turbulence, when the effect of cylindrical geometry vanishes. To this end, Taylor expansions of Eqs. (14) and (15) are given as

$$h_{in} = \alpha_{in}A_T gt^2 - \frac{(\alpha_{in}A_T gt^2)^2}{3r_0} + \cdots + \frac{(-1)^{m-1}r_0}{2(2m)!}\left(\frac{4\alpha_{in}A_T gt^2}{r_0}\right)^m + \cdots, \tag{16}$$

and

$$h_{out} = \alpha_{out}A_T gt^2 + \frac{(\alpha_{out}A_T gt^2)^2}{3r_0} + \cdots + \frac{r_0}{2(2m)!}\left(\frac{4\alpha_{out}A_T gt^2}{r_0}\right)^m + \cdots, \tag{17}$$

where m is the ordinal number corresponding to the mth term a_m of the Taylor series of Eqs. (16) and (17) at a given moment t. As the limits $\lim_{m\to\infty} |a_{m+1}/a_m| = \lim_{m\to\infty} (4\alpha_i A_T gt^2)/[(2m+2)(2m+1)r_0] = 0$, the above series converge according to the D'Alembert's test. Moreover, the difference between the cylindrical and planar cases appears as the curvature effect

$1/r_0$ at the cylindrical interface. The effect of cylindrical geometry will be negligible as $r_0 \to \infty$ and consequently the term $(\alpha_{in}A_T gt^2)/r_0$ is infinitesimal at any given moment t, thus Eqs. (16) and (17) are reduced as $h_{in} = \alpha_{in}A_T gt^2$ and $h_{out} = \alpha_{out}A_T gt^2$. The reduced mixing width is formulated exactly the same as that of planar RT turbulence [5,7]. This

analysis further confirms that our scaling law of mixing layer is valid for cylindrical RT turbulence and transcends the classical power law for the planar RT turbulence.

V. CONCLUSIONS

The scaling laws of the mixing layer in cylindrical RT turbulence are proposed based on physical insights and verified by DNS of the Navier-Stokes equations. Specifically, the outward mixing layer satisfies the hyperbolic cosine growth and the inward mixing layer obeys the cosine growth in cylindrical geometry. The scaling laws for the cylindrical RT turbulence can be recovered to the power law for planar RT turbulence as cylindrical geometry effect vanishes. According to the scaling laws, characteristic time- and length scales are also obtained to describe the self-similar evolution features of the mixing layer in cylindrical RT turbulence. Moreover, we have numerically revealed the multiscale feature and self-similarity and analyzed the fundamental measurements of cylindrical RT turbulence.

[1] Lord Rayleigh, Investigation of the character of the equilibrium of an incompressible heavy fluid of variable density, Proc. Lond. Math. Soc. **s1-14**, 170 (1883).

[2] G. I. Taylor, The instability of liquid surfaces when accelerated in a direction perpendicular to their planes. I, Proc. Roy. Soc. Lond. Ser. A. **201**, 192 (1950).

[3] J. Nuckolls, L. Wood, A. Thiessen, and G. Zimmerman, Laser compression of matter to super-high densities: Thermonuclear (CTR) applications, Nature (Lond.) **239**, 139 (1972).

[4] V. N. Gamezo, A. M. Khokhlov, E. S. Oran, A. Y. Chtchelkanova, and R. O. Rosenberg, Thermonuclear supernovae: Simulations of the deflagration stage and their implications, Science **299**, 77 (2003).

[5] Y. Zhou, Rayleigh–Taylor and Richtmyer–Meshkov instability induced flow, turbulence, and mixing. I, Phys. Rep. **720-722**, 1 (2017).

[6] Y. Zhou, Rayleigh–Taylor and Richtmyer–Meshkov instability induced flow, turbulence, and mixing. II, Phys. Rep. **723-725**, 1 (2017).

[7] D. L. Youngs, Numerical simulation of turbulent mixing by Rayleigh–Taylor instability, Physica D **12**, 32 (1984).

[8] J. R. Ristorcelli and T. T. Clark, Rayleigh–Taylor turbulence: Self-similar analysis and direct numerical simulations, J. Fluid Mech. **507**, 213 (2004).

[9] A. W. Cook, W. Cabot, and P. L. Miller, The mixing transition in Rayleigh–Taylor instability, J. Fluid Mech. **511**, 333 (2004).

[10] M. J. Andrews and D. B. Spalding, A simple experiment to investigate two-dimensional mixing by Rayleigh–Taylor instability, Phys. Fluids A **2**, 922 (1990).

[11] G. Dimonte, Spanwise homogeneous buoyancy-drag model for Rayleigh–Taylor mixing and experimental evaluation, Phys. Plasmas **7**, 2255 (2000).

[12] D. H. Olson and J. W. Jacobs, Experimental study of Rayleigh–Taylor instability with a complex initial perturbation, Phys. Fluids **21**, 034103 (2009).

[13] B. Akula, P. Suchandra, M. Mikhaeil, and D. Ranjan, Dynamics of unstably stratified free shear flows: An experimental investigation of coupled Kelvin–Helmholtz and Rayleigh–Taylor instability, J. Fluid Mech. **816**, 619 (2017).

[14] C. Cherfils and K. O. Mikaelian, Simple model for the turbulent mixing width at an ablating surface, Phys. Fluids **8**, 522 (1996).

[15] A. W. Cook and P. E. Dimotakis, Transition stages of Rayleigh–Taylor instability between miscible fluids, J. Fluid Mech. **443**, 69 (2001).

[16] W. H. Cabot and A. W. Cook, Reynolds number effects on Rayleigh–Taylor instability with possible implications for type Ia supernovae, Nat. Phys. **2**, 562 (2006).

[17] W. Cabot and Y. Zhou, Statistical measurements of scaling and anisotropy of turbulent flows induced by Rayleigh-Taylor instability, Phys. Fluids **25**, 015107 (2013).

[18] D. L. Youngs, The density ratio dependence of self-similar Rayleigh–Taylor mixing, Phil. Trans. R. Soc. A **371**, 20120173 (2013).

[19] Y. Zhou and B. Thornber, A comparison of three approaches to compute the effective Reynolds number of the implicit large-eddy simulations, J. Fluids Eng. **138**, 070905 (2016).

[20] Z. Zhao, N.-S. Liu, and X.-Y. Lu, Kinetic energy and enstrophy transfer in compressible Rayleigh–Taylor turbulence, J. Fluid Mech. **904**, A37 (2020).

[21] D. Besnard, The megajoule laser program-ignition at hand, Eur. Phys. J. D **44**, 207 (2007).

[22] A. Caproni, G. A. Lanfranchi, A. L. da Silva, and D. Falceta-Gonçalves, Three-dimensional hydrodynamical simulations of the supernovae-driven gas loss in the dwarf spheroidal galaxy ursa minor, Astrophys. J. **805**, 109 (2015).

[23] S. T. Weir, E. A. Chandler, and B. T. Goodwin, Rayleigh–Taylor Instability Experiments Examining Feedthrough Growth in an Incompressible, Convergent Geometry, Phys. Rev. Lett. **80**, 3763 (1998).

[24] K.-G. Zhao, C. Xue, L.-F. Wang, W.-H. Ye, J.-F. Wu, Y.-K. Ding, W.-Y. Zhang, and X.-T. He, Thin shell model for the nonlinear fluid instability of cylindrical shells, Phys. Plasmas **25**, 092703 (2018).

[25] J. P. Sauppe, S. Palaniyappan, J. L. Kline, K. A. Flippo, O. L. Landen, D. Shvarts, S. H. Batha, P. A. Bradley, E. N. Loomis, B. J. Tobias *et al.*, Design of cylindrical implosion experiments to demonstrate scale-invariant Rayleigh–Taylor instability growth, High Energy Dens. Phys. **36**, 100831 (2020).

[26] W. W. Hsing, C. W. Barnes, J. B. Beck, N. M. Hoffman, D. Galmiche, A. Richard, J. Edwards, P. Graham, S. Rothman, and B. Thomas, Rayleigh–Taylor instability evolution in ablatively driven cylindrical implosions, Phys. Plasmas **4**, 1832 (1997).

[27] L.-F. Wang, J.-F. Wu, W.-H. Ye, W.-Y. Zhang, and X.-T. He, Weakly nonlinear incompressible Rayleigh–Taylor instability growth at cylindrically convergent interfaces, Phys. Plasmas **20**, 042708 (2013).

[28] K. O. Mikaelian, Rayleigh–Taylor and Richtmyer–Meshkov instabilities and mixing in stratified cylindrical shells, Phys. Fluids **17**, 094105 (2005).

[29] H.-D. Yu and D. Livescu, Rayleigh–Taylor instability in cylindrical geometry with compressible fluids, Phys. Fluids **20**, 104103 (2008).

[30] C. C. Joggerst, A. Nelson, P. Woodward, C. Lovekin, T. Masser, C. L. Fryer, P. Ramaprabhu, M. Francois, and G. Rockefeller, Cross-code comparisons of mixing during the implosion of dense cylindrical and spherical shells, J. Comput. Phys. **275**, 154 (2014).

[31] J. P. Sauppe, S. Palaniyappan, B. J. Tobias, J. L. Kline, K. A. Flippo, O. L. Landen, D. Shvarts, S. H. Batha, P. A. Bradley, E. N. Loomis, N. N. Vazirani, C. F. Kawaguchi, L. Kot, D. W. Schmidt, T. H. Day, A. B. Zylstra, and E. Malka, Demonstration of Scale-Invariant Rayleigh–Taylor Instability Growth in Laser-Driven Cylindrical Implosion Experiments, Phys. Rev. Lett. **124**, 185003 (2020).

[32] Z. Zhao, P. Wang, N. Liu, and X. Lu, Analytical model of nonlinear evolution of single-mode Rayleigh–Taylor instability in cylindrical geometry, J. Fluid Mech. **900**, A24 (2020).

[33] X. Bian, H. Aluie, D.-X. Zhao, H.-S. Zhang, and D. Livescu, Revisiting the late-time growth of single-mode Rayleigh–Taylor instability and the role of vorticity, Physica D **403**, 132250 (2020).

[34] A. Hillier, Self-similar solutions of asymmetric Rayleigh–Taylor mixing, Phys. Fluids **32**, 015103 (2020).

[35] X. Qiu, Y.-L. Liu, and Q. Zhou, Local dissipation scales in two-dimensional Rayleigh–Taylor turbulence, Phys. Rev. E **90**, 043012 (2014).

[36] Z.-X. Hu, Y.-S. Zhang, B.-L. Tian, Z.-W. He, and L. Li, Effect of viscosity on two-dimensional single-mode Rayleigh–Taylor instability during and after the reacceleration stage, Phys. Fluids **31**, 104108 (2019).

[37] A. Bakhsh, S. Gao, R. Samtaney, and V. Wheatley, Linear simulations of the cylindrical Richtmyer–Meshkov instability in magnetohydrodynamics, Phys. Fluids **28**, 034106 (2016).

[38] M. Lombardini, D. I. Pullin, and D. I. Meiron, Turbulent mixing driven by spherical implosions. Part 1. Flow description and mixing-layer growth, J. Fluid Mech. **748**, 85 (2014).

[39] S. Gauthier, Compressible Rayleigh–Taylor turbulent mixing layer between Newtonian miscible fluids, J. Fluid Mech. **830**, 211 (2017).

[40] P. E. Dimotakis, The mixing transition in turbulent flows, J. Fluid Mech. **409**, 69 (2000).

[41] Y. Zhou, Unification and extension of the similarity scaling criteria and mixing transition for studying astrophysics using high energy density laboratory experiments or numerical simulations, Phys. Plasmas **14**, 082701 (2007).

[42] Y. Zhou, W. H. Cabot, and B. Thornber, Asymptotic behavior of the mixed mass in Rayleigh–Taylor and Richtmyer–Meshkov instability induced flows, Phys. Plasmas **23**, 052712 (2016).

[43] G. Boffetta and A. Mazzino, Incompressible Rayleigh–Taylor turbulence, Annu. Rev. Fluid Mech. **49**, 119 (2017).